Contrib. Astron. Obs. Skalnaté Pleso **44**, 43 – 60, (2014)

Inferring spectral characteristics of the Hα spectral line observed by the DOT Lyot filter

J. Koza, J. Rybák, P. Gömöry and A. Kučera

Astronomical Institute of the Slovak Academy of Sciences
059 60 Tatranská Lomnica, The Slovak Republic, (E-mail: koza@astro.sk)

Received: December 30, 2013; Accepted: April 17, 2014

Abstract. A tunable Lyot filter can serve as a spectroscopic device rendering wide-field 2-D pseudospectroscopy of solar structures and follow-up crude reconstruction of a spectral line profile at each pixel within the field of view. We developed a method of inferring of the Doppler shift, the core intensity, the core width, and the core asymmetry of the Hα spectral line observed by the Lyot filter installed on the Dutch Open Telescope (DOT). The spectral characteristics are inferred through the fitting of five intensity samples, separated from each other by 0.35 Å, by a 4^{th}-order polynomial, a Gaussian, and a parabola. We use the atlas Hα profile as a reference in estimating deviations of the derived spectral characteristics. The Gaussian is the most preferable means for measurements of the Doppler shift with deviations smaller than $1\,\mathrm{km\,s^{-1}}$. When using the 4^{th}-order polynomial, deviations are within the interval $\pm 2.5\,\mathrm{km\,s^{-1}}$, but it renders comparable deviations of the core intensity and the width as the Gaussian. The deviations are largely insensitive to the shape of the filter transmission, but depend mostly non-linearly on the Doppler shift. Therefore, they do not cancel out if the spectral characteristics are represented by their relative variations. Results can be used as corrections of spectral characteristics extracted from area-averaged Hα profiles acquired by the DOT Lyot filter.

Key words: Sun: chromosphere – Line: profiles – Techniques: spectroscopic – Instrumentation: miscellaneous – Methods: miscellaneous

1. Introduction

Since its invention by Lyot (1933) and independently by Öhman (1938), the Lyot filter, called also the Lyot-Öhman filter, the birefringent filter, or less frequently the polarization-interference monochromator (Stix, 2004), has earned broad utilization as an imaging device in quasi-monochromatic wide-field surveys of the solar atmosphere. Its employment as a spectroscopic device was severely limited by fast seeing variations in tuning from one wavelength setting to another. Only the advent of the adaptive optics, the image reconstruction, and space-based observatories enabled to overcome effectively this difficulty and to extend usage of a tunable Lyot filter also in wide-field 2-D pseudospectroscopy of solar structures in two or more wavelengths in a spectral line profile. Subsequently, the filtergrams obtained at multiple wavelengths allow constructing of subtractive

Dopplergrams (Tsiropoula, 2000; Rutten *et al.*, 2008; Kontogiannis *et al.*, 2010) as well as to perform a crude reconstruction of a spectral line profile and to derive its spectral characteristics at each pixel within a field of view through a curve fitting of profile samples either with a parabola (Sütterlin *et al.*, 2001; de Wijn *et al.*, 2009) or a Gaussian (Jess *et al.*, 2009).

However, a few-point sampling of a spectral line profile with a very low spectral resolution evokes a question of an accuracy of extracted spectral characteristics. In general, an application of a Lyot filter together with a curve fitting may alter original characteristics to some extent. It is desirable to know a quantitative estimate of this alteration. In this context, Shchukina *et al.* (2009) performed a detailed analysis of the NLTE formation of the Ba II 4554 Å spectral line using a snapshot from a 3-D hydrodynamical simulation of the solar photosphere and low chromosphere with the aim of studying correspondence between the vertical velocities in the snapshot and the velocities obtained from a parabolic fit of five samples across synthetic Ba II 4554 Å profiles as it would be observed through a Lyot filter equivalent to the Irkutsk barium birefringent filter (Skomorovsky *et al.*, 1976; Kushtal, Skomorovsky 2002; Hammerschlag *et al.*, 2010) installed on the Dutch Open Telescope (hereafter DOT; Hammerschlag, Bettonvil 1998; Bettonvil *et al.*, 2003; Rutten *et al.*, 2004).

An aim of this study is to estimate deviations of the Doppler shift, the core intensity, the core width, and the core asymmetry of the Hα spectral line observed by the DOT Hα Lyot filter (Gaizauskas, 1976; Bettonvil *et al.*, 2006) assuming two different transmission profiles. The spectral characteristics are derived using a 4^{th}-order-polynomial, a Gaussian, and a parabolic fit of five samples of the Hα profile extracted from the spectral atlas (Neckel, 1999) and shifted within the velocity range $\pm 25\,\mathrm{km\,s^{-1}}$. The study compares these three curves in terms of deviations of measured spectral characteristics and examines whether the deviations are sensitive to the shape of the filter transmission profile.

A possible application of results of this study is in interpreting Hα images available in the DOT open database[1] searchable through its search engine[2]. Currently, the database contains at least 15 time sequences taken in the quiet Sun at the position angle θ with $\mu = \cos\theta > 0.7$ between 14 October 2005 and 28 September 2007 sampling the Hα profile at $\Delta\lambda = 0, \pm 0.35$, and ± 0.7 Å around its center. These sequences can be converted into spectral characteristics using results of this study. It is possible that the database will later be supplemented with Hα time sequences obtained after 2007 since the DOT Hα data taken in 2010 have already appeared in Rutten & Uitenbroek (2012), Joshi et al. (2013), Panasenco et al. (2014), and in the poster presentation by Aparna, Hardersen & Martin at the meeting of the Solar Physics Division of the American Astronomical Society in 2013.

[1] `http://dotdb.strw.leidenuniv.nl/DOT/`

[2] `http://dotdb.strw.leidenuniv.nl/search/`

2. Convolved intensity and transmission profiles

The convolved intensity $E(\lambda)$ of incident light with a spectrum I passing through a filter with a transmission profile T centered at the wavelength λ is the convolution

$$E(\lambda) = \int_0^\infty I(x)T(x-\lambda)dx\,. \tag{1}$$

For an application of a Lyot filter as a spectroscopic device and follow-up quantitative interpretation of observed $E(\lambda)$, *e.g.*, through comparison with a synthetic spectrum I, one needs to assume or to know the transmission profile T and its possible variations with tuning of the filter. This is also needed for the aims of this study given in the introduction.

Thorough investigation of the transmission profile of the DOT Hα Lyot filter was performed in Koza *et al.* (2014) resulting in a model of the profile approximated by a square of a normalized sinc function in the form

$$\mathrm{sinc}^2(\Delta\lambda) = \left(\frac{\sin \pi x}{\pi x}\right)^2, \tag{2}$$

where $x = 2k\frac{\Delta\lambda}{\mathrm{FWHM}}$, $k = 0.442946$, $\Delta\lambda$ is the distance from the center of the passband, and FWHM is the full width at half maximum of the profile central peak equal to 250 mÅ. The sinc^2 function is supplemented with two rectangle functions Π centered at $\Delta\lambda = \pm 2$ Å around the Hα line center with an area of 11.5 mÅ each (width = 107 mÅ, height = 0.107). This combined model of the transmission T_1 of the DOT Hα Lyot filter is henceforth referred to as $\mathrm{sinc}^2 + \Pi$. We employ also another model T_2 represented by a Gaussian with FWHM = 250 mÅ. These two models allow us to assess how a choice of a particular model of transmission influences the estimated deviations of the spectral characteristics mentioned in the introduction. To avoid an awkward unit of the convolved intensity $E(\lambda)$ in application of Eq. (1), area-normalized transmission profiles T_1 and T_2 in units of inverse wavelength are commonly used to yield $E(\lambda)$ in the same units as I. Hereafter, referring to the $\mathrm{sinc}^2 + \Pi$ and Gaussian transmission profile means their area-normalized versions.

3. Method, spectral characteristics, and references

As a reference, we adopt the disk-center Hα profile taken from the spectral atlas (Neckel, 1999). The profile is shifted using Doppler velocities within the interval $\pm 25\,\mathrm{km\,s^{-1}}$ with a step of $1\,\mathrm{km\,s^{-1}}$. The interval was chosen to embrace Doppler shifts found in the chromospheric network in our preliminary analysis of the DOT Hα dataset from 19 October 2005 and also the shock velocities found in the numerical simulations by Heggland *et al.* (2011). Then each of the 51 profiles is convolved with five Gaussian and $\mathrm{sinc}^2 + \Pi$ transmission profiles located at $0, \pm 0.35$, and ± 0.7 Å from center of the atlas Hα profile. The resulting five

convolved intensities $E(\lambda)$ are fitted by a $4^{\rm th}$-order polynomial, a Gaussian, and a parabola. For the polynomial and parabola fitting the IDL function `poly_fit` was used and for the Gaussian the IDL `gaussfit` function (Figs. 1 – 3). The former performs a least-square polynomial fit using matrix inversion to determine the polynomial or parabola coefficients. The latter calls the IDL function `curvefit`, which uses a gradient-expansion algorithm to compute a non-linear least squares fit to a user-supplied function. Then we determine the core intensity $I_{\rm C}$ and Doppler shift $v_{\rm C}$ of the fit minima with respect to the center of the atlas profile expressed in velocity units while the positive Doppler shift corresponds to redshift. Although $I_{\rm C}$ and relevant intensities are derived from the convolved intensities $E(\lambda)$, we indicate them in the following as I supplemented with an appropriate *ad hoc* subscript.

Missing continuum intensity measurements near the Hα line preclude estimating the full width at half minimum $fwhm$ of the original profile. To guess its core width from the convolved intensities, we introduce the fit width FW as the wavelength separation of the two opposite flanks of the line core fit at the average intensity $I_{\rm FW}$ defined as

$$I_{\rm FW} = (I_{\rm RF} + I_{\rm C})/2\,, \tag{3}$$

where $I_{\rm RF}$ is the reference intensity, substituting the missing continuum intensity, and $I_{\rm C}$ is the core intensity of the fit. We adopt a subscript $_{\rm FW}$ associating the average intensity with the fit width measurement. Similarly to Cauzzi *et al.* (2009), we define the reference intensity $I_{\rm RF}$ as

$$I_{\rm RF} = (I_{-0.6} + I_{+0.6})/2\,, \tag{4}$$

where $I_{-0.6}$ and $I_{+0.6}$ are fit intensities at the wavelength separation of ± 0.6 Å from the wavelength of the fit minimum. Examples of the convolved intensities, trinity of fit functions, their extrapolations, and average intensities $I_{\rm FW}$ for the Gaussian fit and the Gaussian transmission profile are displayed in Fig. 1 for the redshifts of $+15$ and $+10\,{\rm km\,s^{-1}}$ in the top and bottom panel, respectively. The same is in Fig. 2, but for the $\mathrm{sinc}^2 + \Pi$ profile and the blueshifts of -25 and $-21\,{\rm km\,s^{-1}}$ in the top and bottom panel, respectively. Fits of highly Doppler-shifted profiles may have the average intensities larger than the minimum of the observed endpoint intensities, *i.e.*, $I_{\rm FW} > \min(I_{-0.7}, I_{+0.7})$, examples of which is the top panel of Fig. 1 and both panels of Fig. 2. In such cases, the fit width FW is determined by fit extrapolations (shown in gray). Notice undulation and local maxima of the $4^{\rm th}$-order polynomial (Fig. 1, the bottom panel of Fig. 2) and failure of the parabolic fit for large Doppler shifts (Fig. 2). We emphasize that large Doppler shifts selected for Figs. 1 and 2 are extremely rare in the chromosphere. Results by Cauzzi *et al.* (2009) show that most of the Hα Doppler shifts in the quiet-Sun chromosphere are within the range $\pm 5\,{\rm km\,s^{-1}}$. Thus Fig. 3 illustrates fits occurring in most of chromospheric profiles with Doppler shifts up to $\pm 5\,{\rm km\,s^{-1}}$. One can notice that convolved intensities are perfectly fitted by

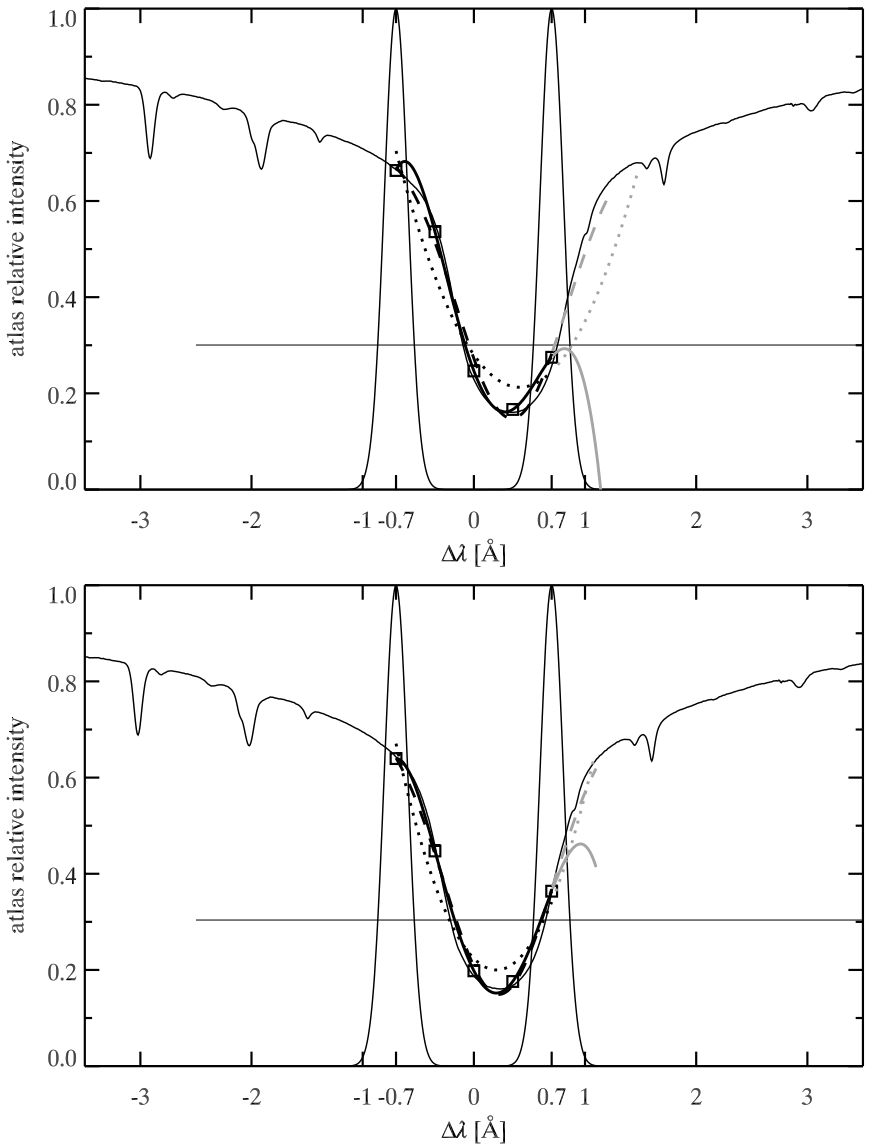

Figure 1. Examples of the convolved intensities (squares) obtained from the atlas Hα profile (thin solid) redshifted by about $+15\,\mathrm{km\,s^{-1}}$ (top) and $+10\,\mathrm{km\,s^{-1}}$ (bottom) and the Gaussian transmission profile with FWHM = 250 mÅ centered at $0, \pm 0.35$, and ± 0.7 Å (the last two shown as thin solid) together with a 4^{th}-order-polynomial (thick solid), Gaussian (dashed), and parabolic (dotted) fit and their extrapolations (gray) beyond 0.7 Å. The horizontal line indicates the average intensity I_{FW} (Eq. 3) for the Gaussian fit.

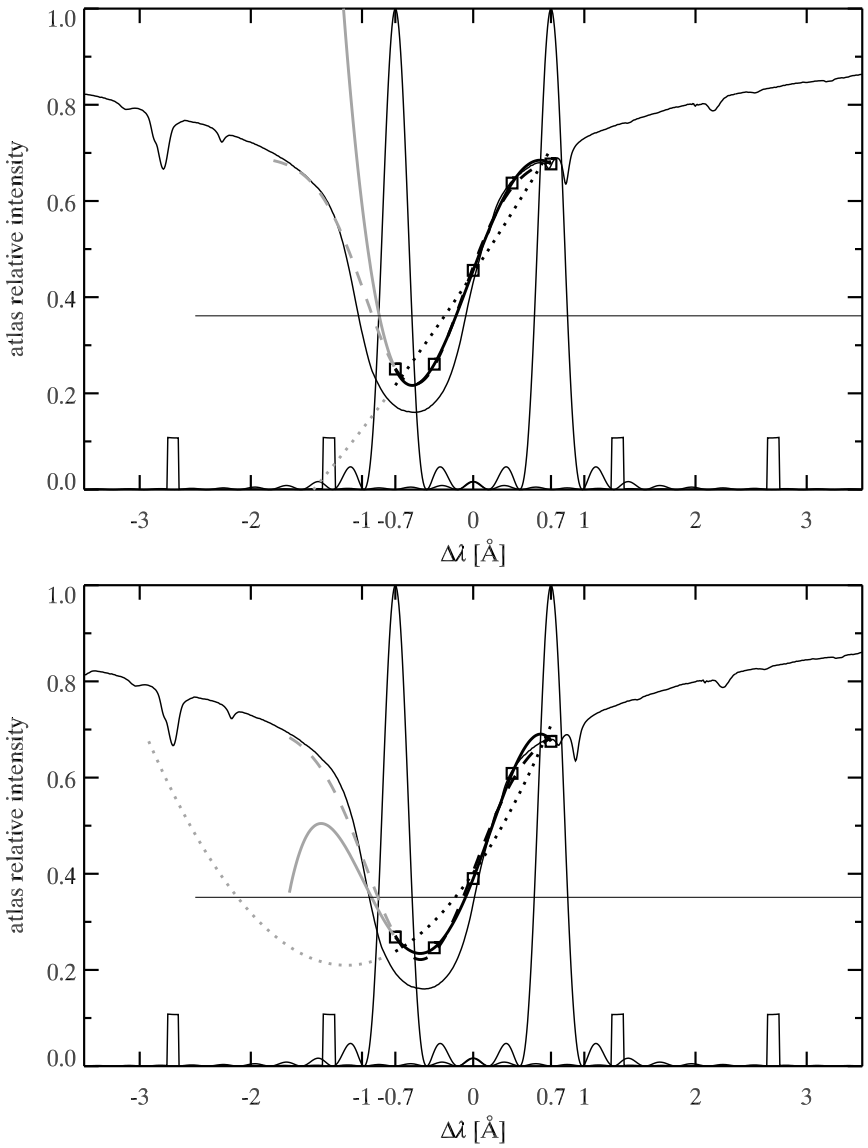

Figure 2. The same as in Fig. 1, but for the atlas Hα profile blueshifted by about $-25\,\mathrm{km\,s^{-1}}$ (top) and $-21\,\mathrm{km\,s^{-1}}$ (bottom) and the $\mathrm{sinc}^2 + \Pi$ transmission profile. Gray lines indicate fit extrapolations beyond -0.7 Å.

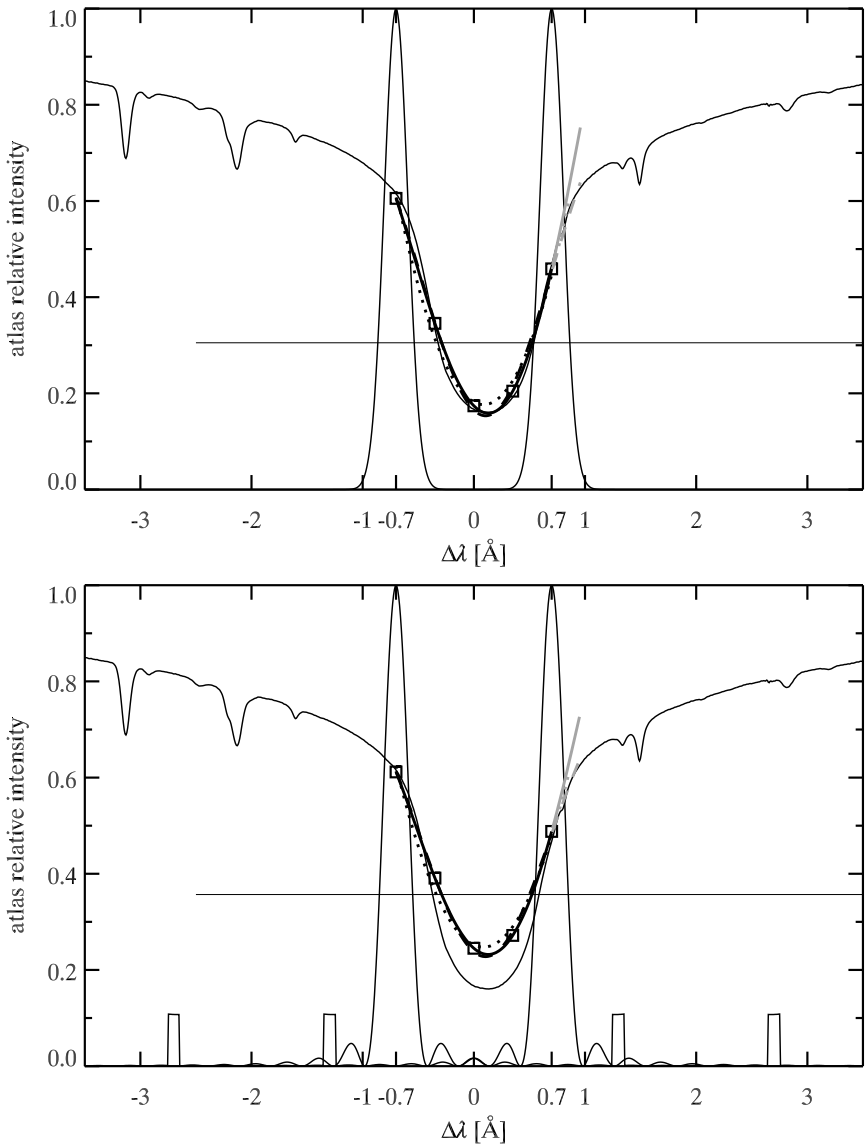

Figure 3. Top: The same as in Fig. 1, but for the atlas Hα profile redshifted about $5\,\mathrm{km\,s^{-1}}$. Bottom: The same as in Fig. 2, but for the atlas Hα profile redshifted about $5\,\mathrm{km\,s^{-1}}$.

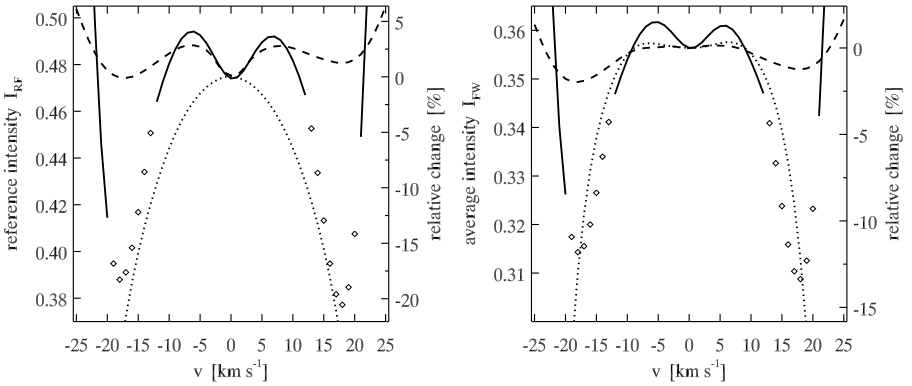

Figure 4. The reference intensity I_{RF} (the left panel, Eq. 4), the corresponding average intensity I_{FW} (the right panel, Eq. 3), and their relative changes (right ordinates) *versus* the Doppler shift of the atlas Hα profile for a 4^{th}-order-polynomial (solid), Gaussian (dashed), and parabolic (dotted) fit of convolved intensities. The diamonds indicate values estimated by the spline interpolation of discontinuities of the solid curves caused by undulation of the 4^{th}-order polynomial.

both the 4^{th}-order polynomial and the Gaussian, but only the polynomial gives a possibility to estimate an asymmetry of the Hα core. On the other hand, the parabolic function yields less satisfactory fits than the two former curves even at these low Doppler shifts. For simplification of the text and plots, all following figures display results pertinent only to the $\mathrm{sinc}^2 + \Pi$ transmission profile.

A special attention deserves variability of the reference I_{RF} and average intensity I_{FW} (Eqs. 3 and 4) with the Doppler shift of the atlas Hα profile shown in Fig. 4 for the particular fitting curves. The right ordinates show the relative changes of I_{RF} and I_{FW} with respect to their values at $v = 0\,\mathrm{km\,s^{-1}}$. Apparently, the Gaussian fit provides the most stable value of the average intensity I_{FW} (shown as the dashed line) - variations are within the interval $\pm 2\,\%$ in the considered range of Doppler shifts. The average intensity is almost constant for the parabolic fit (dotted) within the interval of Doppler shifts of $\pm 10\,\mathrm{km\,s^{-1}}$. In the same interval, the variations of I_{FW} for the 4^{th}-order-polynomial fit are less than $2\,\%$, but out of it I_{FW} varies wildly for both polynomial fitting curves. The Gaussian transmission profile renders the same figure, but with different ranges on ordinates. The diamonds indicate the values of I_{RF} and I_{FW} estimated by the spline interpolation of discontinuities in solid curves due to undulation of the 4^{th}-order polynomial occurring at large Doppler shifts.

We tested also another possible definition of the reference intensity given as $(I_{-0.7} + I_{+0.7})/2$, where $I_{-0.7}$ and $I_{+0.7}$ are observed endpoint intensities at $\Delta\lambda = \pm 0.7\,\text{Å}$ from the zero wavelength. However, this approach proved to

be a much less convenient proxy for the missing continuum intensities than the definition in Cauzzi *et al.* (2009) adopted for this study. This is because the definition based on intensities at ± 0.7 Å makes a strong link between the Doppler shift and the resulting reference and average intensities which decrease systematically with an increasing Doppler shift. It shifts measurement of the fit width into lower and narrower portions of the fit. In this respect, the definition introduced in Cauzzi *et al.* (2009) provides more stable values of I_{RF} and I_{FW} at least within the range of Doppler shifts of $\pm 10\,\mathrm{km\,s^{-1}}$.

We pursue in this study with the 4^{th}-order polynomial because our preliminary analysis of the DOT Hα dataset from 19 October 2005 showed highly asymmetric Hα profiles occurring in the network, which are incompatible with neither a parabola nor a Gaussian. Examples of such profiles occurring at high Doppler shifts are shown in Koza *et al.* (2013) in Fig. 8. The simplest estimate of the asymmetry of the 4^{th}-order polynomial is through a one-point bisector of the line core fit at the average intensity I_{FW}. For this purpose, we introduce the bisector velocity v_{BI} defined as

$$v_{\mathrm{BI}} = c(\lambda_{\mathrm{BI}} - \lambda_{\mathrm{C}})/\lambda_0\,, \tag{5}$$

where c is the speed of light, λ_{BI} is the wavelength of the midpoint of a horizontal chord of the line core fit at I_{FW}, λ_{C} is the wavelength at its core intensity I_{C}, and λ_0 is the wavelength of the intensity minimum of the Hα line of 6562.8 Å. The center of gravity of the line core fit, whose area is limited from the top by the average intensity I_{FW}, renders another estimate of asymmetry. The respective center-of-gravity velocity is defined as

$$v_{\mathrm{COG}} = c(\lambda_{\mathrm{COG}} - \lambda_{\mathrm{C}})/\lambda_0\,, \tag{6}$$

where λ_{COG} is the wavelength of the center of gravity given as

$$\lambda_{\mathrm{COG}} = \frac{\sum\limits_i \lambda_i (I_{\mathrm{FW}} - I_i)}{\sum\limits_i I_{\mathrm{FW}} - I_i}\,, \tag{7}$$

where I_i is the fit intensity at the wavelength λ_i, and the index i runs through all wavelengths with $I_i \leq I_{\mathrm{FW}}$. The sign convention in Eqs. (6) and (7) suggests positive or negative v_{BI} and v_{COG} for a line core fit with a redward or blueward asymmetry, respectively.

Since in the following we aim to estimate the deviations of v_{C}, I_{C}, FW, v_{BI}, and v_{COG} obtained by particular fitting curves, we need to define their reference values considered as precise. Obviously, the reference of v_{C} is the given Doppler shift of the atlas Hα profile referred as v. The reference of I_{C} (I_{r} hereafter) is the intensity minimum of the atlas Hα profile of 0.16 expressed in atlas units of continuum intensity. We adopt as a references of FW (FW_{r} hereafter) the value of 893 mÅ, which is the width of the atlas Hα profile at the

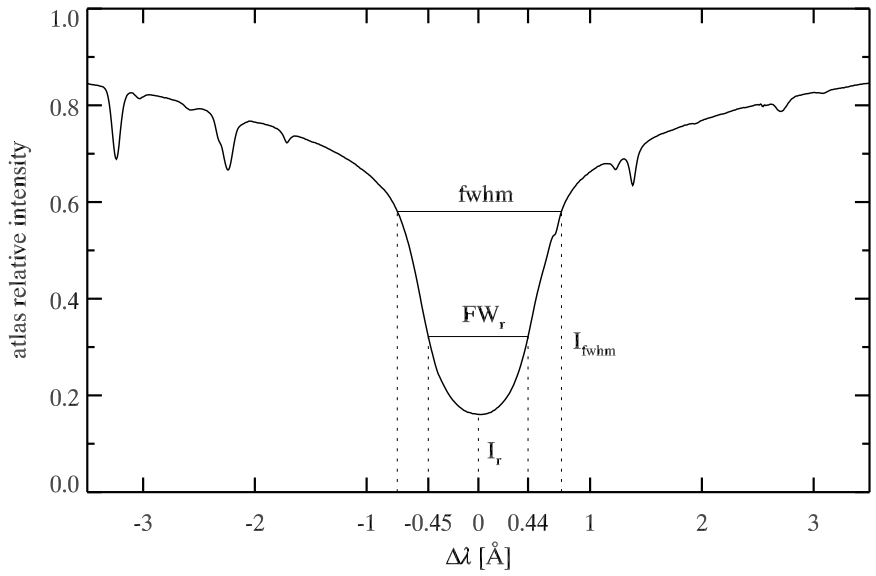

Figure 5. The disk-center Hα profile extracted from the spectral atlas (Neckel, 1999) with indicated intensity minimum $I_\mathrm{r} = 0.16$, the reference for the fit width $FW_\mathrm{r} = 893\,\mathrm{m\AA}$, and the full width at half minimum $fwhm = 1\,469\,\mathrm{m\AA}$.

average intensities of 0.32 computed by Eqs. (3) and (4) with input quantities in atlas units of continuum intensity. Figure 5 illustrates the references I_r and FW_r and relation of the latter with respect to $fwhm$ of 1 469 mÅ computed as the wavelength separation of the two opposite flanks of the profile at the intensity $I_\mathrm{fwhm} = (1 + I_\mathrm{r})/2 = 0.58$.

Finally, with the aim of defining the reference values of v_BI and v_COG, we measured an asymmetry of the bottom tip of the atlas Hα profile by Eqs. (5) – (7) finding the values -98 and $-30\,\mathrm{ms}^{-1}$. Since both are significantly smaller than the spectral sampling of the atlas Hα profile equivalent to $357\,\mathrm{ms}^{-1}$, we adopt zero as the reference values of v_BI and v_COG referred to in the following as r_BI and r_COG.

4. Results

One of the aims of this study defined in the introduction is an examination whether a choice of a particular model of a transmission profile has some influence on the estimated deviations of the spectral characteristics. For this purpose, we used two considerably different models of transition profile of the DOT Hα filter represented by the Gaussian and $\mathrm{sinc}^2 + \Pi$ function. We found out that the deviations are insensitive to the choice of the model. Therefore, in the following

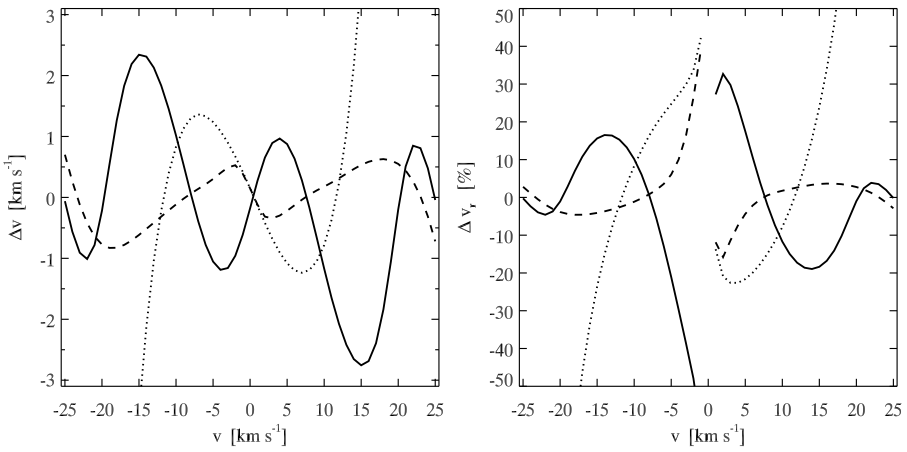

Figure 6. An absolute Δv (left) and relative Δv_r (right) deviation of the measured Doppler shift of a 4^{th}-order-polynomial (solid), Gaussian (dashed), and parabolic (dotted) fit with respect to the reference Doppler shift of the atlas Hα profile v.

we present only results pertinent to the $\mathrm{sinc}^2 + \Pi$ model, but much the same is valid for the Gaussian model of the transmission profile.

The left and right panels of Fig. 6 show the absolute and relative deviations of the Doppler shift v_C defined as $\Delta v = v_\mathrm{c} - v$ and $\Delta v_\mathrm{r} = \Delta v/|v|.100\%$, respectively, for the particular fitting curves. The left panel suggests that the Gaussian fit should be the most preferable choice for measurements of the Doppler shift with deviations less than $1\,\mathrm{km\,s^{-1}}$ within the interval $\pm 25\,\mathrm{km\,s^{-1}}$. In the same interval, an application of a 4^{th}-order-polynomial fit results in considerably variable deviations ranging from -2.5 to $+2.5\,\mathrm{km\,s^{-1}}$. This is also the case of the parabolic fit within the interval of Doppler shifts of $\pm 15\,\mathrm{km\,s^{-1}}$. Out of it, deviations for the parabolic fit grow very steeply because a parabola cannot fit the atlas profile reliably (see Fig. 2). Therefore, deviations of large Doppler shifts v_C derived by the parabolic fit are unknown. The right panel of Fig. 6 shows relative deviations of the Doppler shift Δv_r with respect to the absolute value of the reference Doppler shift $|v|$ of the atlas Hα profile. Clearly, they grow steeply as v approaches zero. For $|v|$ larger than $5\,\mathrm{km\,s^{-1}}$, the Gaussian and the 4^{th}-order-polynomial fits provide Doppler shifts v_C with relative deviations less than 5 % and 20 %, respectively. As explained earlier, the apparent growth of Δv_r for the parabolic fit for $|v| > 15\,\mathrm{km\,s^{-1}}$ is questionable.

The left panel of Fig. 7 shows simultaneously the absolute and relative deviations of the core intensity I_C (the left and right ordinate) defined as $\Delta I = I_\mathrm{c} - I_\mathrm{r}$ in atlas units of continuum intensity and $\Delta I_\mathrm{r} = \Delta I/I_\mathrm{r}.100\%$, respectively, for the particular fitting curves. This common display is allowed by the unique reference value I_r shared by all curves. Obviously, all fitting curves overestimate the core

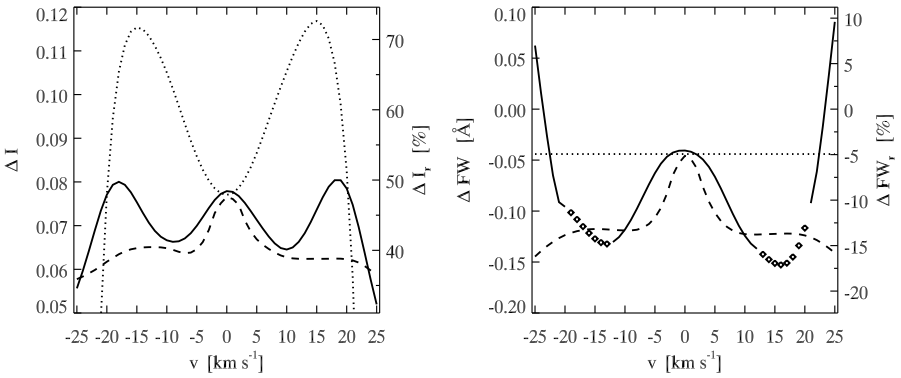

Figure 7. Left: An absolute ΔI and relative $\Delta I_{\rm r}$ deviation of the core intensity (left and right ordinate, respectively) of a $4^{\rm th}$-order-polynomial (solid), Gaussian (dashed), and parabolic (dotted) fit at the reference Doppler shift v with respect to the intensity minimum of the atlas Hα profile. Right: An absolute ΔFW and relative $\Delta FW_{\rm r}$ deviation of the fit width (left and right ordinate, respectively) of a $4^{\rm th}$-order-polynomial (solid), Gaussian (dashed), and parabolic (dotted) fit at the reference Doppler shift v with respect to the reference width of the atlas Hα profile. The diamonds indicate values estimated by the spline interpolation of discontinuities of the solid curve caused by undulation of the $4^{\rm th}$-order polynomial.

intensity due to the effect of integration over the normalized filter transmission profile (Eq. 1). Curves in the left panel of Fig. 7 can be useful for estimating the minimum intensity of the original Hα profile from convolved intensities when normalized to atlas units of continuum intensity. The $4^{\rm th}$-order-polynomial fit overestimates $I_{\rm C}$ with the sinus-like relative deviation varying from 40 to 50%. The Gaussian fit also overestimates the core intensity $I_{\rm C}$ from 40 to 50%, but its deviations are almost constant for Doppler shifts larger than $5\,{\rm km\,s^{-1}}$. Therefore, they cancel out if $I_{\rm C}$ is expressed as relative variations with respect to its mean value. The parabolic fit overestimates $I_{\rm C}$ from 50 to 70% within the interval of Doppler shifts of $\pm 15\,{\rm km\,s^{-1}}$. Out of it, estimating ΔI is impossible because a parabola cannot fit the atlas profile reliably for Doppler shifts out of the interval $\pm 15\,{\rm km\,s^{-1}}$ (see Fig. 2).

Similarly to the left one, the right panel of Fig. 7 shows simultaneously the absolute and relative deviations of the fit width FW (the left and right ordinate) defined as $\Delta FW = FW - FW_{\rm r}$ and $\Delta FW_{\rm r} = \Delta FW/FW_{\rm r}.100\%$, respectively, for the particular fitting curves. All fitting curves underestimate the fit width from -0.05 up to $-0.15\,$Å, *i.e.*, from -5 to -15%. Surprisingly, the parabolic fit exhibits a constant underestimate of FW about -5% and also the Gaussian fit displays an almost constant underestimate about -14% for Doppler shifts larger

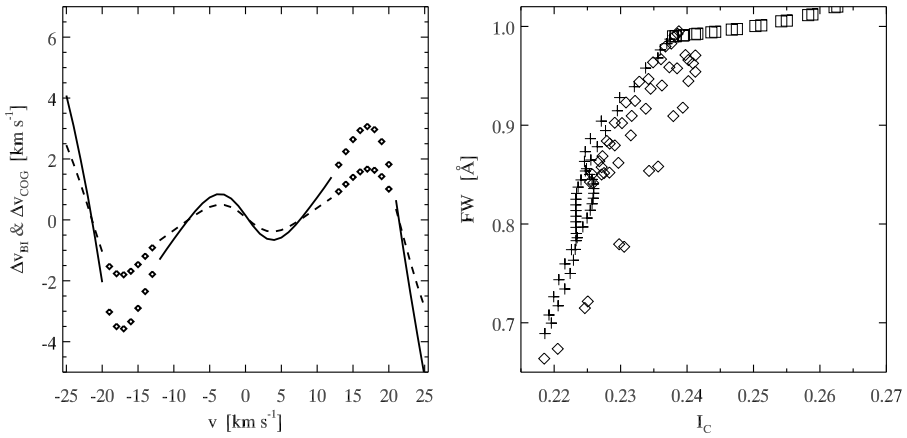

Figure 8. Left: An absolute deviation of the bisector $\Delta v_{\rm BI}$ (solid) and the center-of–gravity $\Delta v_{\rm COG}$ (dashed) velocity of a $4^{\rm th}$-order-polynomial fit with respect to their zero reference values. The diamonds indicate values estimated by the spline interpolation of discontinuities of curves caused by undulation of the $4^{\rm th}$-order polynomial. Right: Artificial correlations of the fit width FW and the core intensity $I_{\rm C}$ for a $4^{\rm th}$-order-polynomial (diamonds), Gaussian (plus signs), and parabolic (squares) fit.

than $5\,{\rm km\,s^{-1}}$. As in the case of $I_{\rm C}$, if FW is expressed as relative variations with respect to its mean value than the constant underestimates cancel out.

The left panel of Fig. 8 shows only the absolute deviations of the bisector and the center-of-gravity velocity defined as $\Delta v_{\rm BI} = v_{\rm BI} - r_{\rm BI}$ and $\Delta v_{\rm COG} = v_{\rm COG} - r_{\rm COG}$, respectively, for the $4^{\rm th}$-order-polynomial fit. The deviations are within the interval $\pm 1\,{\rm km\,s^{-1}}$ for Doppler shifts smaller than $5\,{\rm km\,s^{-1}}$. But for larger Doppler shifts, the deviations are exceedingly large compared to the adopted zero reference values of $r_{\rm BI}$ and $r_{\rm COG}$ (see the last paragraph of Section 3) suggesting that the five-point sampling of the Hα line profile is too coarse and insufficient for a meaningful estimate of the core asymmetry for Doppler shifts larger than $5\,{\rm km\,s^{-1}}$. The diamonds in the right and left panels of Figs. 7 and 8, respectively, indicate deviations of FW, $v_{\rm BI}$, and $v_{\rm COG}$ estimated by the spline interpolation of the pertinent curves due to undulation of the $4^{\rm th}$-order polynomial occurring at large Doppler shifts.

Finally, dependencies of $I_{\rm C}$ and FW on the Doppler shift v (Fig. 7) results in an artificial FW – $I_{\rm C}$ correlation shown in the right panel of Fig. 8. Similar figure renders also the Gaussian transmission profile. The dependence is apparent for the $4^{\rm th}$-order-polynomial (diamonds) and the Gaussian (plus signs) fits, suggesting that deeper fits are narrower and *vice versa*, shallower fits are wider. The correlation seems to be negligible for the parabolic fit. Similar artificial correlations are foreseeable for pairs of other quantities.

5. Application

This section outlines an application of previous results in correcting the measured Doppler shift d, core intensity i, fit width f, bisector velocity b, or center-of-gravity velocity c inferred from a DOT Hα dataset, taken in the quiet Sun near the disk center. We assume a sampling of the Hα profile at $\Delta\lambda = 0, \pm 0.35$, and ± 0.7 Å around its center and a fitting of five measured intensities either with a 4^{th}-order polynomial, or a Gaussian, or a parabola. Then the corrected Doppler shift D is the solution of the transcendental equation

$$\Delta v(D) + D - d = 0\,, \tag{8}$$

where the function $\Delta v(D)$ corresponds to the absolute deviations of the Doppler shift shown in the left panel of Fig. 6. Since the function Δv is not continuous but a set of discrete values defined for particular Doppler shifts v from the interval $\pm 25\,\mathrm{km\,s^{-1}}$, Eq. (8) can be rewritten as

$$\texttt{interpol}(\Delta v, v, D) + D - d = 0\,, \tag{9}$$

where `interpol` is the respective IDL function. Equation (9) can be solved numerically, *e.g.*, by the IDL function `fx_root`. Consequently, the corrected core intensity I, fit width F, bisector velocity B, and center-of-gravity velocity C result directly from the equations

$$I = i - \texttt{interpol}(\Delta I, v, D)\,, \tag{10}$$

$$F = f - \texttt{interpol}(\Delta FW, v, D)\,, \tag{11}$$

$$B = b - \texttt{interpol}(\Delta v_{\mathrm{BI}}, v, D)\,, \tag{12}$$

$$C = c - \texttt{interpol}(\Delta v_{\mathrm{COG}}, v, D)\,, \tag{13}$$

where ΔI, ΔFW, Δv_{BI}, and Δv_{COG} are the absolute deviations displayed in Fig. 7 and the left panel of Fig. 8 interpolated on the grid of corrected Doppler shifts D.

6. Discussion

In this study, we estimated deviations of spectral characteristics derived by fitting five samples of the atlas Hα profile inferred through its convolution with two models of the transmission profile of the DOT Hα Lyot filter shifted within the interval $\pm 25\,\mathrm{km\,s^{-1}}$. We found that the deviations are largely insensitive to the shape of two transmission profiles employed and the choice of the fitting curve is more important. Therefore, for any real transmission profile of the DOT Hα Lyot filter, the results shown in Figs. 6 – 8 can be applied as corrections of spectral characteristics as described in the previous section. In the following, we compare pros and cons of particular fitting curves.

The Gaussian fit delivers measurements of the Doppler shift with the smallest deviations not exceeding $1\,\mathrm{km\,s^{-1}}$ (Fig. 6). Deviations of its core intensity I_C and fit width FW do not vary much for Doppler shifts larger than $5\,\mathrm{km\,s^{-1}}$ (Fig. 7) and, therefore, can be eliminated by commonly used relative variations. But so high Doppler shifts are rather rare in the chromosphere (Cauzzi *et al.*, 2009). Therefore, most of values of I_C and FW should be corrected in the way described in the previous section. We encountered only a practical drawback of the IDL function `gaussfit`, which needs a good initial estimate of Gaussian parameters, otherwise the IDL function `curvefit` does not converge within 20 iterations set as default. Sometimes setting more than 20 iterations is needed for its convergence.

So far rarely used the 4^{th}-order-polynomial fit delivers comparable deviations of I_C and FW as the Gaussian fit (Fig. 7). Its deviations of the Doppler shift are somewhat larger than those rendered by the Gaussian fit (Fig. 6), but contrary to a parabola, these are limited and defined within the whole interval $\pm 25\,\mathrm{km\,s^{-1}}$. However, a main technical difficulty in application of the 4^{th}-order-polynomial fit is its undulation at large Doppler shifts and an occurrence of local maxima (Figs. 1 and 2). On the other hand, this curve allows estimating an asymmetry of a sufficiently sampled Hα profile. As we pointed out in the last but one paragraph of Section 4, the five-point sampling is far from optimum. Therefore, the results shown in the left panel of Fig. 8 are only rough corrections for a better estimate of the bisector and center-of-gravity velocities.

An easy application of the parabolic fit is its main advantage comparing to other two fitting curves. Within the interval of Doppler shifts of $\pm 15\,\mathrm{km\,s^{-1}}$ it delivers similar deviations of the Doppler shift as the two others (Fig. 6). However, the applied method does not allow to make a realistic estimate of the deviations within the whole interval $\pm 25\,\mathrm{km\,s^{-1}}$ and their apparent steep growth out of the interval $\pm 15\,\mathrm{km\,s^{-1}}$ is questionable. Curiously, the parabolic fit yields the smallest and constant deviations of the fit width ΔFW over the whole interval of Doppler shifts (the right panel of Fig. 7) albeit it shows the least satisfactory match of the convolved intensities (Figs. 1 and 3).

7. Recommendation, applicability, and upgraded method

We have been forced to introduce the reference intensity I_{RF} in Eq. (3) as a proxy for the missing continuum intensity. Therefore, we recommend to include at least one continuum intensity measurement near Hα in future observations aiming to estimate its $fwhm$ by a Fabry-Pérot instrument or a Lyot filter as in Jess *et al.*, (2009). However, it is unclear how far from the line center one needs to tune the passband to reach a proper continuum near the Hα spectral line (Fig. 5). To avoid extrapolations in an $fwhm$ estimate, we recommend also to include two far-wing measurements at ± 1.5 Å. Thus, an optimum sampling

of the Hα profile by a Lyot filter suitable for its $fwhm$ estimate would be: continuum, $\pm 1.5, \pm 0.7, \pm 0.35$, and 0 Å.

We used the atlas Hα profile shifted in the range $\pm 25\,\mathrm{km\,s^{-1}}$ as a reference. In other words, we considered a one-parametric case when the deviations Δv, ΔI, ΔFW, Δv_{BI}, and Δv_{COG} in Figs. 6 – 8 are solely due to the Doppler shift of an otherwise unchanged reference profile. Of course, compared with reality, this may be considered as a highly unrealistic and oversimplified approach, or even a serious shortcoming, since Doppler shifts of spectrally, spatially, and temporally resolved on-disk Hα profiles are accompanied with their asymmetries and shape variability (see, *e.g.*, Cauzzi *et al.*, 2009). Nevertheless, we consider our results as useful for applications dealing with Hα profiles taken with a low spectral, spatial, and/or temporal resolution. This is just the case of Hα profile samples taken by a Lyot filter and spatially averaged over some area smoothing out the shape oddities (see Koza *et al.*, 2013 and Fig. 9 therein).

Anyhow, we outline here an upgraded multi-parametric method accounting for them. It consists in obtaining long-slit high-resolution Hα spectra taken over an extensive quiet-Sun area in the disk center at many slit positions as an ample source of reference Hα profiles of high shape variability. In the next, a set of reference spectral characteristics will be inferred from each reference profile. Then the reference profiles will be convolved with several settings of the transmission profile of a Lyot filter and resulting convolved intensities will be fitted with a selected curve. As an outcome, a set of measured spectral characteristics will be derived from each fit. Thus, the method will yield an extensive lookup table relating reference spectral characteristics, considered as true, with their measured counterparts resulting from the combination of a particular filter, a frequency of profile sampling, and a fitting curve. The method can even provide a relation between FW and $fwhm$ (Fig. 5). At this point, we leave unanswered a question of practical implementation of such lookup table in correcting the measured spectral characteristics.

8. Conclusions

The study introduces a method of inferring spectral characteristics from five intensity samples of the Hα spectral line observed by the DOT Lyot filter. To compensate for the limited spectral resolution through the curve fitting, we estimated deviations of the spectral characteristics using the atlas Hα profile as a reference and suggested a correcting procedure. The deviations are largely insensitive to the shape of filter transmission, but the choice of the fitting curve is more important. They depend mostly non-linearly on the Doppler shift and, therefore, they do not cancel out if the characteristics are represented by their relative variations as is commonly used. Our results suggest that the Gaussian fit should be the most preferable means for measurements of the Doppler shift with deviations smaller than $1\,\mathrm{km\,s^{-1}}$ within the velocity interval $\pm 25\,\mathrm{km\,s^{-1}}$.

Deviations of the Doppler shift of the 4^{th}-order-polynomial fit are within the interval $\pm 2.5\,\mathrm{km\,s^{-1}}$, but it renders comparable deviations of the core intensity and the fit width as the Gaussian. Moreover, the former allows estimating the asymmetry of the line core for sufficiently sampled profiles. But, as we have shown, the five-point sampling is far from optimum since the estimated deviations of the bisector and center-of-gravity velocities are exceedingly large and their corrected values should be considered with caution. The main technical difficulty in usage of the 4^{th}-order polynomial is its undulation at large Doppler shifts. Otherwise, in terms of deviations, it is almost equivalent to or better than the Gaussian or the parabola. Conclusively, our results shown in Figs. 6 – 8 can be applied as corrections of spectral characteristics extracted from area-averaged Hα profiles acquired by a Lyot filter with FWHM = 250 mÅ tuned at $\Delta\lambda = 0, \pm 0.35$, and ± 0.7 Å around the Hα line center.

Acknowledgements. The authors are grateful to P. Schwartz for his thorough review of the paper which improved its clarity. This work was supported by the Slovak Research and Development Agency under the contract No. APVV-0816-11. This work was also supported by the Science Grant Agency - project VEGA 2/0108/12.

References

Bettonvil, F.C.M., Hammerschlag, R.H., Sütterlin, P., Rutten, R.J., Jägers, A.P.L., Sliepen, G.: 2006, in *Proc.: Ground-based and Airborne Instrumentation for Astronomy*, eds.: Ian S. McLean and Masanori Iye, SPIE Conf. Series, Orlando, Florida, USA, Vol. 6269

Bettonvil, F.C., Sütterlin, P., Hammerschlag, R.H., Jagers, A.P., Rutten, R.J.: 2003, in *Proc.: Innovative Telescopes and Instrumentation for Solar Astrophysics*, eds.: Stephen L. Keil and Sergey V. Avakyan, SPIE Conf. Series, Waikoloa, Hawai'i, USA, Vol. 4853, pp. 306-317

Cauzzi, G., Reardon, K., Rutten, R.J., Tritschler, A., Uitenbroek, H.: 2009, *Astron. Astrophys.* **503**, 577

de Wijn, A.G., McIntosh, S.W., De Pontieu, B.: 2009, *Astrophys. J., Lett.* **702**, L168

Gaizauskas, V.: 1976, *J. R. Astron. Soc. Can.* **70**, 1

Hammerschlag, R.H., Bettonvil, F.C.M.: 1998, *New Astronomy Reviews* **42**, 485

Hammerschlag, R.H., Skomorovsky, V.I., Bettonvil, F.C.M., Kushtal, G.I., Olshevsky, V.L., Rutten, R.J., Jägers, A.P.L., Sliepen, G., Snik, F.: 2010, in *Proc.: Ground-based and Airborne Instrumentation for Astronomy III*, eds.: Ian S. McLean, Suzanne K. Ramsay and Hideki Takami, SPIE Conf. Series, San Diego, California, USA, Vol. 7735

Heggland, L., Hansteen, V.H., De Pontieu, B., Carlsson, M.: 2011, *Astrophys. J.* **743**, 142

Jess, D.B., Mathioudakis, M., Erdélyi, R., Crockett, P.J., Keenan, F.P., Christian, D.J.: 2009, *Science* **323**, 1582

Joshi, A.D., Srivastava, N., Mathew, S.K., Martin, S.F.: 2013, *Sol. Phys.* **288**, 191

Kontogiannis, I., Tsiropoula, G., Tziotziou, K., Georgoulis, M.K.: 2010, *Astron. Astrophys.* **524**, A12

Koza, J., Hammerschlag, R.H., Rybák, J., Gömöry, P., Kučera, A., Schwartz, P.: 2014, *Astron. Nachr.* **335**, 409
Koza, J., Sütterlin, P., Gömöry, P., Rybák, J., Kučera, A.: 2013, *Contrib. Astron. Obs. Skalnaté Pleso* **43**, 5
Kushtal, G.I., Skomorovsky, V.I.: 2002, in *Proc.: Seventh International Symposium on Laser Metrology Applied to Science, Industry, and Everyday Life*, eds.: Yuri V. Chugui, Sergei N. Bagayev, Albert Weckenmann and P. Herbert Osanna, SPIE Conf. Series, Novosibirsk, Russia, Vol. 4900, pp. 504
Lyot, B.: 1933, *Comptes Rendus Acad. Sci.* **197**, 1593
Neckel, H.: 1999, *Sol. Phys.* **184**, 421
Öhman, Y.: 1938, *Nature* **141**, 157
Panasenco, O., Martin, S.F., Velli, M.: 2014, *Sol. Phys.* **289**, 603
Rutten, R.J., Hammerschlag, R.H., Bettonvil, F.C.M., Sütterlin, P., de Wijn, A.G.: 2004, *Astron. Astrophys.* **413**, 1183
Rutten, R.J., Uitenbroek, H.: 2012, *Astron. Astrophys.* **540**, A86
Rutten, R.J., van Veelen, B., Sütterlin, P.: 2008, *Sol. Phys.* **251**, 533
Shchukina, N.G., Olshevsky, V.L., Khomenko, E.V.: 2009, *Astron. Astrophys.* **506**, 1393
Skomorovskij, V.I., Merkulenko, V.E., Polyakov, V.I.: 1976, *Byulletin Solnechnye Dannye Akademie Nauk SSSR* **5**, 73
Stix, M.: 2004, *The sun: an introduction, 2nd ed.*, Springer, Berlin
Sütterlin, P., Rutten, R.J., Skomorovsky, V.I.: 2001, *Astron. Astrophys.* **378**, 251
Tsiropoula, G.: 2000, *New Astron.* **5**, 1